International Journal of GEOMATE, June, 2024 Vol.26, Issue 118, pp.105-113
ISSN: 2186-2982 (P), 2186-2990 (O), Japan, DOI: https://doi.org/10.21660/2024.118.4451
Geotechnique, Construction Materials and Environment

POROTHERMOELASTIC MODEL FOR ANALYSIS OF STRESS STATE AROUND WELLBORES IN ANISOTROPIC ROCK

*Tran Nam Hung[1], Pham Duc Tiep[1], Nguyen Van Hieu[1]

[1] Institute of Technique for Special Engineering, Le Quy Don Technical University, Vietnam

*Corresponding Author, Received: 20 Feb. 2024, Revised: 12 March 2024, Accepted: 14 March 2024

ABSTRACT: Analyzing the stress state around wellbores, and thereby the safe mud pressure window, is an indispensable task in the design as well as assessment of wellbore stability. As considering a realistic behavior model of materials, distributions in the literature mainly referred to the development of analytical or numerical calculation models without mentioning the stress state around the wellbore related to the form of well wall instability. This study aims to analyze the stress state of the rock mass around the wellbore in a homogenous porothermoelastic anisotropic rock based on the finite element method. Two scenarios involving thermal conditions at the well wall are taken into account, i.e. cases of "cooling" and "heating" the wellbore. The coupled thermo-hydro-mechanical behavior model of the rock is used to describe instantaneously the thermic, hydraulic, and mechanical processes and their reciprocal interactions. The results showed that the temperature conditions on the well wall strongly affect the stress distribution around the wellbore, and thereby the stability of the well wall. For the cooling case, the compressive stress around the well wall is not large, but high tensile stress can appear, especially for the axial stress component which can reach 23 MPa. For the heating case, both the compressive tangential and axial stresses with very high values occur around the wellbore ranging from 70-75 MPa. The parametric study showed that the degree of anisotropy of Young's modulus, thermal expansion coefficient, as well as bedding angle of the transversely isotropic rock, strongly affect the stress distribution around the wellbore.

Keywords: Wellbore, Thermo-hydro-mechanical model, Anisotropic rock, Cooling, Heating

1. INTRODUCTION

Wellbores are widely used in the petroleum exploration and production industry, geothermal extraction, underground water extraction, deep geological storage, etc. In such cases, the wellbores can be drilled at great depths where the formation would be saturated and dominated by geothermal phenomena. The temperature of materials underground can reach several hundred degrees [1]. In the design and evaluation of wellbore stability, determining the safe mud pressure window, i.e. the minimum and maximum mud pressures for the well wall to be stable, is essential. This work requires analyzing the stress state of the rock mass surrounding the well wall with different drilling fluid pressures. The calculations of stresses are usually calculated relying on the hypothesis of the homogeneous and isotropic dry rock [1-3]. However, the wellbores are usually built in layers of sedimentary and metamorphic rock that have stratified structures [4-6]. The existence of the stratified structures of the rock leads to an anisotropic response of the rock mass under loading and unloading. It is also the case for the response of rock mass traversed by oriented discontinuities even if the intact rock (without discontinuities) is isotropic. These rocks belong to the transversely isotropic rock class. During drilling the wellbores, if the temperature of the drilling fluid is different from the temperature of the surrounding medium, heat transfer occurs on the well wall. Thus, in this process, thermic, hydraulic, and mechanical phenomena take place simultaneously and interact with each other within the rock.

Recently in the literature, there have been many studies on the stress state of the wellbore. Whilst Kanfar et al. [7], Do et al. [8,9], Tran et al. [10], Khoshghalb [11, 12], Ghaffaripour et al. [13], and Shafee and Khoshghalb [14] relied on the hydro-mechanical behavior model, Abousleiman and Ekbote [15] and Kanfar et al. [16] based on a full thermo-hydro-mechanical behavior model of the materials. However, these works mainly focus on the development of analytical and numerical models without emphasizing the difference in stress state around the wellbore between the cases of cooling and heating as well as different anisotropy degrees of the rocks. It is the stress state around the well wall with the locations of the maximum values of compressive and tensile stresses that can destabilize the well wall in the form of collapse or fracture failures as the stresses in the rock mass exceed its strength.

This paper presents analyses of the stress state around a horizontal wellbore in transversely isotropic rock based on the finite element method. The fully coupled thermo-hydro-mechanical behavior model of the material is used to describe the interaction between the thermic, hydraulic, and mechanical phenomena within the rock. Two scenarios, i.e. heating and cooling cases are considered. Sensitivity analysis is finally carried out to highlight the most significant key parameters controlling the stress state on the well wall.

In the following part of the article, the authors will present the research significance, problem description along with constitutive equations and evaluation of the influence of different parameters on the stress state around the wellbore.

2. RESEARCH SIGNIFICANCE

This study aims to analyze the stress state of the rock mass around the wellbore in a homogenous porothermoelastic anisotropic rock with two scenarios involving thermal conditions at the well wall, i.e. the cooling and heating the wellbore, respectively. The study emphasizes the fundamental difference in stress states between the two scenarios, thereby determining the form of well wall instability that can occur. The influence of different parameters of the anisotropic medium on the stress state around the well is also evaluated.

3. PROBLEM DESCRIPTION AND CONSTITUTIVE EQUATIONS

3.1 Problem Description

A horizontal wellbore of radius r_0 drilled in deep saturated transversely isotropic porous formation is considered in this study. Assume that the rock material is linearly elastic and homogeneous. The Cartesian coordinate system is attached to the wellbore as shown in Fig. 1 with the wellbore axis on the *z*-axis and the wellbore cross-section in the *x*-*y* plane. Because the wellbore is located at a great depth and its diameter is usually small (about tens of centimeters), it can be considered that the wellbore is in an infinite medium. Assuming also that, the initial temperature and pore pressure of the rock mass, i.e. at infinity, are equal to T_{ff} and p_{ff}, respectively; the drilling fluid temperature and pressure at the well wall are T_w and P_w, respectively; the rock bedding angle is β. Since the length of the wellbore is much larger than its diameter, the problem can be studied under the plane strain conditions in the *x*-*y* plane.

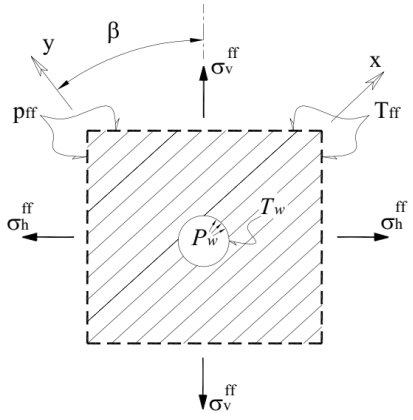

Fig. 1 The horizontal wellbore drilled in a transversely isotropic rock

In reality, the behavior of the geomaterials around the wellbore can be non-linear, and the presence of the wellbore can cause cracks surrounding it. The rock mass can reach a plastic state as pointed out by several authors [13,17,18]. In this study, the behavior of the rock mass is limited to the linear elastic state that is still accepted in many studies in the literature, especially for anisotropic materials [15,16,20].

3.2 Constitutive Equations

All points in the rock mass around the wellbore must satisfy the following basic equations for the plane strain problem in the *x*-*y* plane according to the thermo-hydro-mechanical behavior model.

• Heat transfer and fluid flow equations:

The heat transfer in the rock mass obeys Fourier's law. This law establishes a relationship between temperature variation over time (τ) and space (x, y coordinates) and thermal properties of the material. Meanwhile, the fluid flow obeys Darcy's law. Darcy's law describes the relationship between the pore pressure and hydraulic properties of porous geo-material. For the homogeneous and transversely isotropic material, one has the following differential equations for heat transfer and fluid flow [15,19]:

$$\frac{\partial}{\partial x}\left(\lambda_x^T \frac{\partial T}{\partial x}\right)+\frac{\partial}{\partial y}\left(\lambda_y^T \frac{\partial T}{\partial y}\right)=\rho C_p \frac{\partial T}{\partial \tau} \tag{1}$$

$$\frac{\partial}{\partial x}\left(\lambda_x^F \frac{\partial p}{\partial x}\right)+\frac{\partial}{\partial y}\left(\lambda_y^F \frac{\partial p}{\partial y}\right)=\frac{\partial \chi}{\partial \tau} \tag{2}$$

where λ_x^T and λ_y^T are the heat conductivity coefficients in x and y directions, respectively; λ_x^F and λ_y^F are the hydraulic conductivities in x and y directions, respectively; ρ is the density of the geo-material; C_p is the specific heat of the rock; χ is the change of pore fluid volume per unit volume of the material.

The "bulk heat capacity", ρC_p, can be related to individual heat capacities of the solid and fluid constituents by [11]:

$$\rho C_p=(1-\phi)\rho^s C_p^s+\phi\rho^f C_p^f \tag{3}$$

in which the superscripts *s* and *f* refer to the solid and fluid, respectively.

The heat conductivity coefficient of a saturated porous geo-material is determined according to the heat conductivity coefficients of its phases as follows:

$$\lambda^T=(1-\phi)\lambda_s^T+\phi\lambda_f^T \tag{4}$$

where $\lambda^T{}_s$ and $\lambda^T{}_f$ stand for the heat conductivity coefficients of the solid and liquid phases, respectively, and ϕ is the rock's porosity. The

hydraulic conductivity is related to the intrinsic permeability of the material (K^F_{int}) according to the following expression:

$$\lambda^F = \frac{K^F_{\text{int}}}{\mu_f} \tag{5}$$

with m_f the viscosity of the fluid.

• The equilibrium equations are written in the *x*-*y* plane:

$$\frac{\partial \sigma_x}{\partial x} + \frac{\partial \tau_{xy}}{\partial y} = 0; \qquad \frac{\partial \tau_{yx}}{\partial x} + \frac{\partial \sigma_y}{\partial y} = 0 \tag{6}$$

where σ_x, σ_y, τ_{xy} are the normal stresses in *x*, *y* directions and shear stress in *x*-*y* plane, respectively.

• The strain compatibility equation in the *x*-*y* plane:

$$2\frac{\partial^2 \varepsilon_{xy}}{\partial x \partial y} = \frac{\partial^2 \varepsilon_x}{\partial y^2} + \frac{\partial^2 \varepsilon_y}{\partial x^2} \tag{7}$$

where ε_x, ε_y, ε_{xy} are the normal strains in *x*, *y* directions and shear strain in *x*-*y* plane, respectively.

• The thermo-elastic equation of saturated porous materials for the plane strain problem:

$$\begin{pmatrix} \varepsilon_x \\ \varepsilon_x \\ \varepsilon_{xy} \end{pmatrix} = \begin{pmatrix} s_{11} & s_{12} & 0 \\ s_{21} & s_{22} & 0 \\ 0 & 0 & s_{33} \end{pmatrix} \left[\begin{pmatrix} \sigma_x \\ \sigma_y \\ \tau_{xy} \end{pmatrix} + \begin{pmatrix} b_x \\ b_y \\ 0 \end{pmatrix} p \right] + \begin{pmatrix} \alpha^s_x \\ \alpha^s_y \\ 0 \end{pmatrix} T \tag{8}$$

where α^s_x, α^s_y are the thermal expansion coefficients of the solid phase in *x* and *y* directions, respectively; *T* is the temperature variation within the rock at the point considered; s_{ij} are the components of the compliance tensor of the material; b_x, b_y are the Biot coefficients in *x* and *y* directions, respectively.

• The effective stresses based on Biot's theory are determined from the total stresses and pore pressure by:

$$\sigma'_x = \sigma_x + b_x p, \quad \sigma'_y = \sigma_y + b_y p \tag{9}$$

Note also that in Eq. (9) the tensile stress and pore pressure are considered positive.

4. NUMERICAL EXAMPLE

The numerical example in this study is a horizontal wellbore drilled at a depth of 4000 m below the earth's surface with a radius r_0=0.1 m. The properties of shale [16,20] are used with parameters and drilling fluid temperature, drilling fluid pressure, and initial stress field are given in Table 1.

The geometry model and boundary conditions of the problem are illustrated in Fig. 2. The distance from the wellbore center in the vertical and horizontal directions to the outer boundaries is 100 times the wellbore radius. With respect to this distance, the wellbore is considered to be in an infinite medium, and it can be considered that the entire medium before drilling the wellbore is dominated by uniform initial stress and pore pressure fields.

Table 1 Values of parameters used in numerical simulation

Parameters	Unit	Values
Young modulus in *x* direction, E_x	GPa	28.97
Young modulus in *y* direction, E_y	GPa	24.14
Poisson ratio in anisotropic plane, ν_{xy}	-	0.24
Poisson ratio in the isotropic plane, ν_{xz}	-	0.3
Principle initial stresses in the cross-section σ_h, σ_v	MPa	-25; -30
Solid thermal expansion coefficient in *x* direction, α^s_x	1/K	21.6×10^{-6}
Solid thermal expansion coefficient in *y* direction, α^s_y	1/K	18×10^{-6}
Fluid thermal expansion coefficient, α^f	1/K	3×10^{-4}
Solid thermal conductivity in *x* direction, λ^T_{sx}	$W.m^{-1}.K^{-1}$	1.56
Solid thermal conductivity in *y* direction, λ^T_{sy}	$W.m^{-1}.K^{-1}$	1.3
Fluid thermal conductivity, λ^T_f	$W.m^{-1}.K^{-1}$	0.586
Solid specific heat capacity, C^s_p	$J.kg^{-1}.K^{-1}$	768
Fluid specific heat capacity, C^f_p	$J.kg^{-1}.K^{-1}$	4181
Intrinsic permeability in *x* direction, K^{int}_x	darcy	22.98×10^{-8}
Intrinsic permeability in *y* direction, K^{int}_y	darcy	7.66×10^{-8}
Fluid viscosity, μ_f	Pa.s	3×10^{-4}
Fluid bulk modulus, K_f	GPa	2.30
Biot coefficient in *x* direction, b_x	-	0.72
Biot coefficient in *y* direction, b_y	-	0.76
Porosity, ϕ	-	0.1
Solid matrix density, ρ_s	kg/m^3	2640
Fluid density, ρ_f	kg/m^3	1113

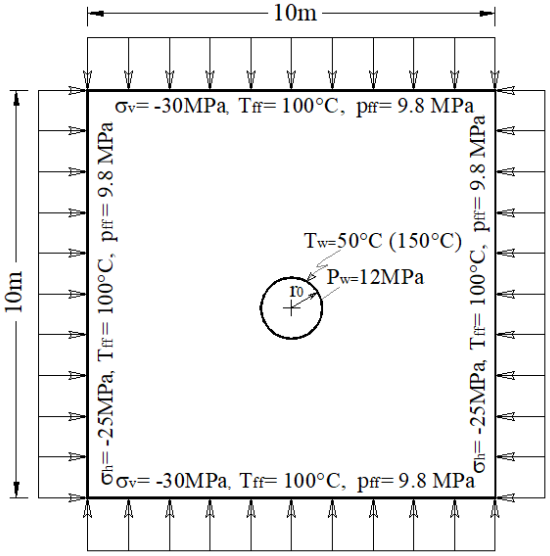

Fig. 2 Geometry model and boundary conditions

In the numerical simulation, the eight nodal quadratic plane strain finite elements are chosen and the well-wall arc is discrete into 200 elements.

In order to evaluate the influence of drilling fluid temperature on the stress state around the wellbore, two numerical simulation scenarios were performed. The first case considers the drilling fluid temperature (50°C) to be below the initial temperature of the rock mass (100°C), referred to as "cooling". The second scenario corresponds to the case where the drilling fluid temperature is above the initial rock mass temperature, referred to as "heating". This heating scenario is usually the result of the drilling fluid having a history of passing through the rock that is hotter than the studied rock, i.e. it has received an amount of heat from the previous rock mass.

In this study, the authors use the finite element method to solve the problem under the multi-physical thermo-hydro-mechanical behavior of the material. The calculations will be made based on the open-source code, Aster, developed by the French Electricity Corporation (EDF) [21]. The validation of the numerical model implemented in the code was presented in [22]. This code built on the Galerkin variational principle was originally developed to analyze hydroelectric dams subjected to earthquake loads and nuclear reactors with the molten core, which require very high accuracy. Later, the code was developed to analyze various multi-physical behaviors and was used by a large number of European scientists.

5. RESULTS AND DISCUSSION

5.1 Effect of Cooling and Heating on The Stress Distribution Around the Wellbore

Figures 3 and 4 show the change in temperature and pore pressure of the rock mass around the wellbore over time for the two scenarios. It can be seen that, in the first case, because the temperature of the drilling fluid is lower than the initial temperature of the rock mass, the rock mass temperature around the wellbore decreases over time. Meanwhile, the temperature evolution tends to be opposite in the latter case where the drilling fluid temperature is greater than the initial temperature of the rock mass. Concerning the pore pressure, in the first case, it decreases strongly in the vicinity of the well wall and in early times when the rock mass is in contact with the drilling fluid. This phenomenon occurs because the liquid phase has a higher thermal expansion coefficient than the one of the solid phase. In the second scenario, in contrast to the previous case, the pore pressure adjacent to the well wall increases greatly, exceeding both the initial pore pressure and drilling fluid pressure. This is due to the larger thermal expansion coefficient of the fluid phase than the one of the solid phase which increases the pore pressure as the temperature increases. Moreover, because the formation has a very low permeability, the pore pressure cannot be dissipated over time under the influence of high temperature. According to Biot's theory, the excess pore water pressure zone around the wellbore will have a great effect on the stress-strain state of the rock mass.

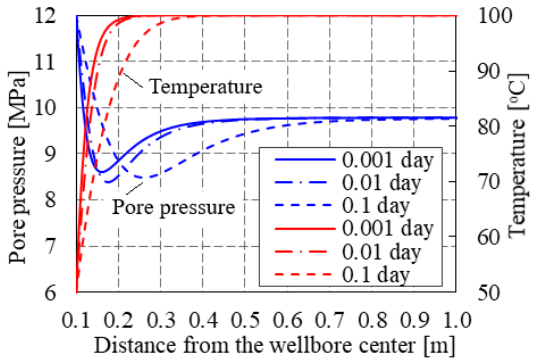

Fig. 3 Evolution of temperature and pore pressure over early time in cooling case

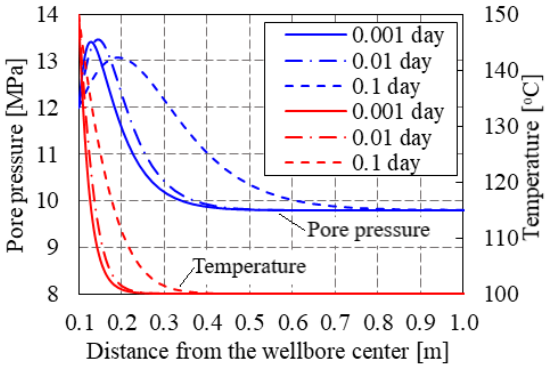

Fig. 4 Evolution of temperature and pore pressure over early time in heating case

Figures 5 and 6 are plots of the effective radial, tangential, and axial stresses with time on a cut inclined at an angle of 45° to the horizontal and passing through the center of the wellbore. It can be seen that the effective radial compressive stress

adjacent to the well wall does not change much through the two cases whereas the tangential and axial effective stresses vary greatly from the cooling case to the heating case. For the cooling case (Fig. 4a), an axial tensile stress region appears in the vicinity of the well wall with a high maximum value (≈16 MPa). This can initiate cracks around the well wall and threaten the wellbore stability if the rock material has low tensile strength. Unlike the cooling case, in the heating case, the tangential compressive effective and axial compressive effective stresses are very high in the vicinity of the well wall. For example, the axial compressive stress reaches a value of approximately 70 MPa while the tangential compressive stress is approximately 76 MPa (Fig. 4b). This shows that the zone adjacent to the well wall can be destabilized if these compressive stress values exceed the compressive strength of the rock. Therefore, the well wall instability can occur under different scenarios depending on the case of the well wall being cooled or heated.

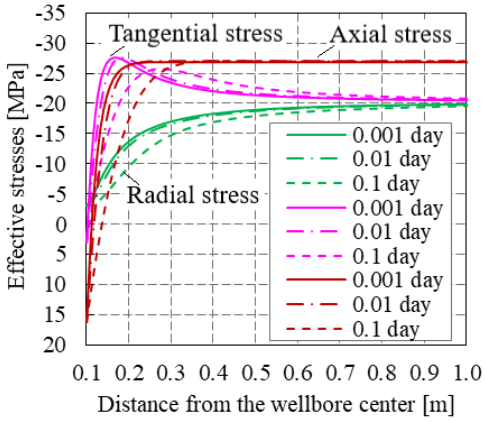

Fig. 5 Stresses over time on the inclined edge in the cooling case

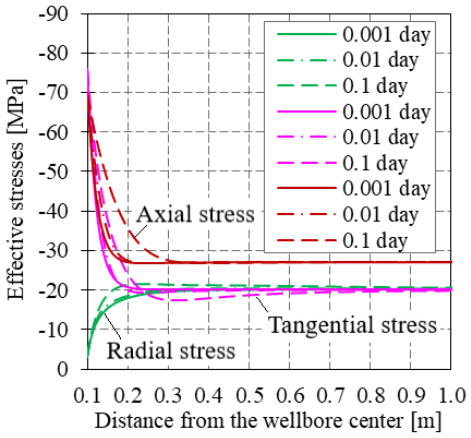

Fig. 6 Stresses over time on the inclined edge in the heating case

To better illustrate the stress distribution on the well wall, Figs. 7 and 8 present the tangential and axial effective stresses along the well wall in comparison with the ones of the wellbore in isotropic rock for the two cases.

For the cooling case, it can be seen that the maximum value of compressive tangential stress appears at the polar angle of 0° and 180° while the one of tensile tangential stress appears at the polar angle of θ=90° and θ=270°. In addition, if comparing the cases of isotropic and anisotropic materials, the value of the minimum compressive tangential stress changes slightly while the value of the maximum tensile tangential stress changes strongly. Concretely, the maximum tangential tensile stress increases from 6.25 MPa to 22.5 MPa (Fig. 7). Meanwhile, the tensile axial stress appears on the entire well wall, and its maximum values are obtained at points with polar angles θ=90° and θ=270°. As passing from isotropic to anisotropic case, the maximum tensile axial stress increases strongly from 8.3 MPa to 22.5 MPa (Fig. 7).

In the literature, many studies have shown that fracture failure around the wellbore will occur when the effective stress on the well wall exceeds the tensile strength of the rock [6,23]. Herein, in the case of cooling, the axial tensile stress distributes in the range of 12-22.5 MPa. This relatively large stress value can cause rock materials with poor tensile strength to crack, thereby causing instability of the well wall.

In the case of heating, the stress distribution along the well wall has an important change compared to the case of cooling. This is a consequence of the difference in thermal boundary conditions of the two scenarios. In particular, the tangential and axial stresses are both compressive and take large values which vary from 68.5 MPa to 76 MPa depending on the location on the well wall (Fig. 8). It should be noted that, if the compressive stresses exceed the material's compressive strength, the well wall may collapse [6,23]. In the cooling case, the extremes of the stresses occur at the same locations as the cooling scenario, i.e. at points with polar angles θ equal to 0°, 90°, 180° and 270°, for both isotropic and anisotropic materials (Fig. 7). Meanwhile, for the anisotropic material, the locations of the extreme points of stresses have changed in the heating scenario. Specifically, the maximum compressive tangential and axial stresses occur about at the polar angles of 45°, 135°, 225° and 315° on the well wall (Fig. 8).

The two scenarios studied above show that, for the cooling scenario, the compressive stress values obtained are not large, but the tensile ones are high (the maximum value of the tensile stress on the well wall reaches approximately 23 MPa); and for the heating scenario, only large compressive stresses are observed (the maximum values of compressive stresses reach 70-76 MPa). To the authors' knowledge, this difference between the two cases could be explained as follows.

In the first scenario, as the well wall is cooled, it contracts and the binding of the neighboring material

causes it to be in tension. The compressive tangential stress zones in this scenario may be due to the fact that the wellbore is also subjected to an anisotropic initial compressive stress field in addition to the cooling. Furthermore, a phenomenon observed is that the tangential tensile stress in the anisotropic material condition is greater than the one in the isotropic material condition. This may be because, in the case of anisotropic rock, the elastic modulus in the horizontal direction (E_x) is larger than that in the vertical direction (E_y) (the value of E_y is also the value of the elastic modulus of the isotropic material in this work). The direction with the larger elastic modulus tends to bear more load.

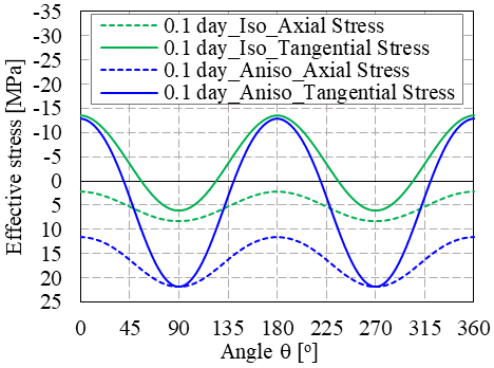

Fig. 7 Stresses on the well wall in the cooling case (t=0.1 day)

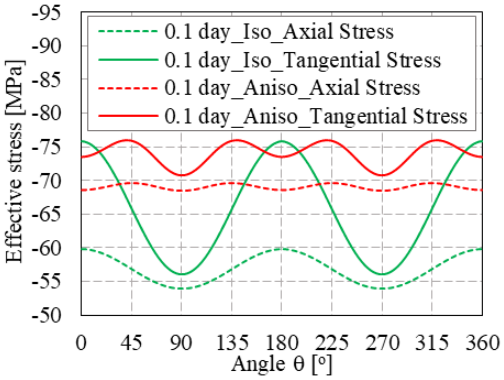

Fig. 8 Stresses on the well wall in the heating case (t=0.1 day)

In the second scenario, as the well wall is heated, the well wall expands. However, the well wall is restricted by the surrounding medium that is subjected to the initial compressive stress field. Thus, compressive stresses always occur on the well wall.

Knowing the stress distribution around the wellbore is important in the wellbore design. Indeed, in the wellbore design, it is first necessary to determine the rock and drilling fluid temperatures at each segment of the wellbore, and then determine the stress state around the well wall corresponding to a certain fluid pressure. This is part of the procedure to determine the minimum and maximum pressures of the drilling fluid, i.e. determination of the safe mud pressure window. As the drilling fluid pressure is outside this pressure range, the well wall can become unstable.

5.2 Effect of Parameters on The Stress Distribution on The Well Wall

In this part, the authors will investigate the effect of the material parameters on the stress distribution on the well wall. Each parameter will be varied while the other parameters are kept constant.

5.2.1 Effect of Young's modulus anisotropy

For the purpose of evaluating Young's modulus anisotropy, one increases Young's modulus in x direction (E_x) by increasing the modulus ratio kE ($kE=E_x/E_y$).

Figures 9 and 10 show the effective stress on the well wall for kE=1.2 (the original case), kE=1.5, and kE=2.0 for the two scenarios.

For the cooling scenario, it can be observed from Fig. 9 that the stresses on the well wall are highly sensitive to the degree of Young's modulus anisotropy, i.e. the higher Young's modulus anisotropy the higher tensile tangential and axial stresses. For example, as kE increases from 1.2 to 1.5, the maximum tensile stress on the well wall increases by about 13 MPa, and as kE increases from 1.5 to 2.0 this quantity increases by 22 MPa. More precisely, as increasing kE rises from 1.2 to 2.0, i.e. by 67%, the maximum tensile stress on the well wall increases from 22 MPa to 57 MPa, an increase of approximately 260%. This shows that the tensile stress is highly sensitive to the degree of anisotropy in terms of Young's modulus.

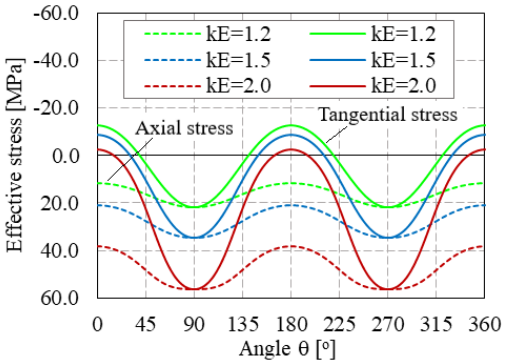

Fig. 9 Stresses on the well-wall with different Young's modulus anisotropy in cooling case (t=0.1 day)

For the heating scenario (Fig. 10), a trend of increase of compressive stresses similar to the one of tensile stresses in the cooling scenario presented above. For instance, as kE increases from 1.2 to 1.5, the maximum compressive tangential stress increases by 12 MPa while the compressive axial stress increases by 13 MPa. As kE increases from 1.5 to 2.0, these quantities increase by 22 MPa and

by 20 MPa, respectively. Thus, if *kE* rises from 1.2 to 2.0, the maximum compressive stress on the well wall increases by an amount of 42% from 76 MPa to 108 MPa.

It should be noted that, in this study, to increase the anisotropy degree, Young's modulus in the *y* direction is kept constant while the one in the *x* direction is increased. As the stiffness in the *x* direction increases, the material would carry more load in this direction where the stiffness is greater.

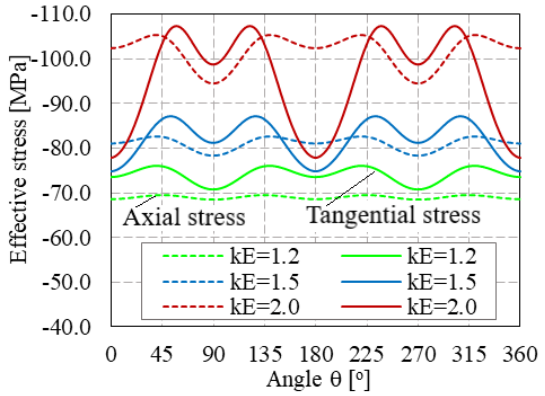

Fig. 10 Stresses on the well-wall with different Young's modulus anisotropy in heating case (t=0.1 day)

5.2.2 Effect of thermic anisotropy

In this estimation, the authors change the degree of thermic anisotropy, which is defined by kAlpha = α_x/α_y, by changing α_x while keeping α_y unchanged. The original case corresponds to kAlpha = 1.2. The results for the cooling and heating scenarios are shown in Figs. 11 and 12.

For the cooling case (Fig. 11), when the α_x increases, i.e. the thermic anisotropy increases, the maximum tensile tangential and axial stresses increase significantly (about 8 MPa) at the polar angle's locations of 90° and 270°, whereas the maximum compressive tangential and axial stresses decrease lightly at the polar angle's locations of 0° and 180°.

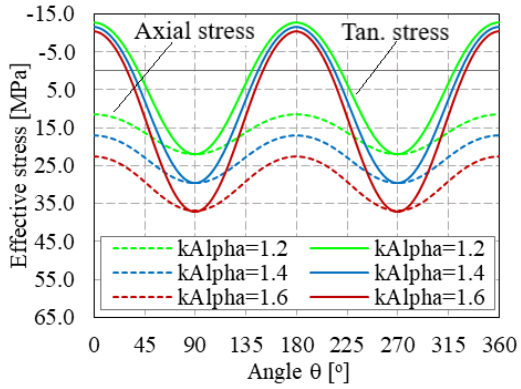

Fig. 11 Stresses on the well wall with different thermic anisotropy in the cooling case (t=0.1 day)

With respect to the heating case (Fig. 12), the higher the thermic anisotropy the higher the maximum compressive tangential and axial stresses. Precisely, the maximum compressive tangential stress increases by about 4.5 MPa and 6 MPa once the degree of thermic anisotropy increases by an amount of 0.2 from 1.2 to 1.6, respectively. Meanwhile, once the degree of thermic anisotropy increases by 0.2, the maximum compressive axial stress increases by about 7 MPa.

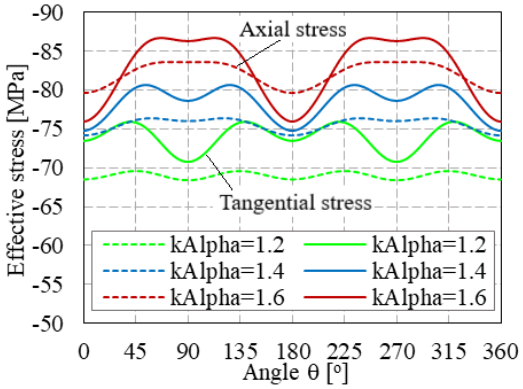

Fig. 12 Stresses on the well wall with different thermic anisotropy in the heating case (t=0.1 day)

5.2.3 Effect of bedding angle

This evaluation presents calculation results with rock bedding angles β equal to 0°, 30°, and 60° (degrees denoted by "d" in the figures), respectively. The results are illustrated in Figs. 13 and 14 for the two scenarios.

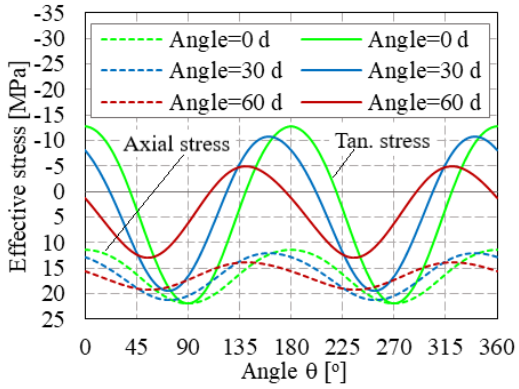

Fig. 13 Stresses on the well wall with different bedding angles in the cooling case (t=0.1 day)

It is observed from Fig. 13 that, in the cooling case, as the bedding angle increases all the maximum compressive, tensile tangential, and axial stresses decrease. In addition, the locations of the stress peaks also change. For example, when changing the bedding angle from 0° to 60°, the polar angle corresponding to the maximum axial stress changes by about 30° while the one corresponding to the maximum tangential stress changes by about 45°.

In contrast to the previous case, in the heating case (Fig. 14), as the bedding angle increases, both the maximum compressive tangential and axial stresses increase. Specifically, as the bedding angle increases from 0° to 60°, the maximum compressive tangential stress increases by about 14 MPa, and the tensile axial stress increases by about 4 MPa. The locations where the maximum tangential and axial stresses occur also change by a polar angle of 30°.

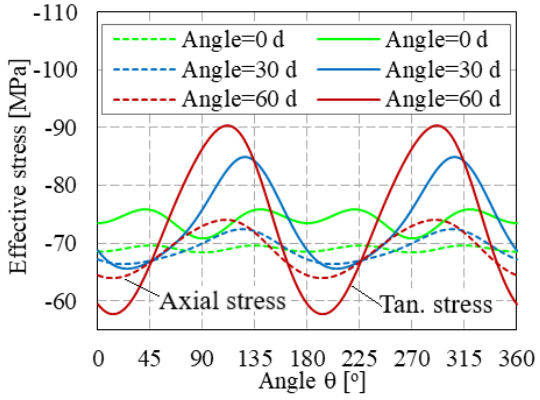

Fig. 14 Stresses on the well wall with different bedding angles in the heating case (t=0.1 day)

6. CONCLUSION

This study is devoted to analyzing the stress state around a horizontal wellbore in an anisotropic porothermoelastic rock based on the finite element method with the coupled thermo-hydro-mechanical behavior model of the material. The following main results can be made.

The multi-physical coupled thermo-hydro-mechanical behavior model of geomaterials is essential to more closely reflect the real working conditions of wellbores drilled in deep geological strata when thermal, hydraulic, and mechanical phenomena occur simultaneously and interact with each other.

The stresses around the wellbore in the anisotropic material are significantly different from the ones of the wellbore in the isotropic material. Therefore, neglecting material anisotropy by assuming an isotropic model will likely yield erroneous results as the rocks exhibit an anisotropic behavior.

The temperature conditions on the well wall strongly influence the stress distribution around the wellbore. For the cooling case, the compressive stress around the well wall is not large, but high tensile stress can appear, especially for the axial stress component. This can lead to damage to the well wall in the form of fracture failure. For the heating case, there are only compressive stresses around the wellbore with very high values. Thus, in this case, the collapse failure of the well wall may occur. Elaborating on how the insights into stress distribution around wellbores can inform better drilling practices, wellbore design, and mitigation strategies for potential failures would be valuable.

The parametric study showed that the degree of anisotropy of Young's modulus, thermal expansion coefficient, and bedding angle of the transversely isotropic rock strongly affect the stress distribution around the wellbore.

This study is limited to the wellbore drilled in the transversely isotropic rock. Stability analysis of the wellbore in an orthotropic rock with anisotropic failure criteria would be an extension of this work in the future.

7. REFERENCES

[1] Zhu Z., Wang C., Guan Z., Lei W., Thermal characteristics of borehole stability drilling in hot dry rock. ACS Omega, ACS Publications, 2021, pp. 19026–19037.

[2] Zhang S., Song H., Chen B., Han C., The development and key drilling technology of hot dry rock in China. Resour. Environ. Eng., 31.2, 2017, pp. 202-207.

[3] Zhou Z., Jin Y., Lu Y., Zhou B., Present challenge and prospects of drilling and hydraulic fracturing technology for hot dry rock geothermal reservoir, Sci. Sin. Phys. Mech. Astron, 48, 2018, 124621.

[4] Amadei B., Rock anisotropy and the theory of stress measurement, Springer,1983, pp. 1-188.

[5] Wittke W., Rock Mechanics Based on an Anisotropic Jointed Rock Model. Wiley, Ernst and Sohn, 2014, pp. 1-90.

[6] Jaeger J.C., Cook N.G.W., Zimmerman R.W., Fundamentals of rock mechanics, 4th edn. Blackwell Publishing, 2007, Oxford, pp. 1-200.

[7] Kanfar, Majed F., Z. Chen, and S. S. Rahman., Effect of material anisotropy on time-dependent wellbore stability, Int J Rock Mech Min Sci, 78, 2015, pp. 36-45.

[8] Do D. P., Tran N. H., Hoxha D. , Dang H. L., Assessment of the influence of hydraulic and mechanical anisotropy on the fracture initiation pressure in permeable rocks using a complex potential approach, Int J Rock Mech Min Sci, 100, 2017, pp. 108–123.

[9] Do D. P., Tran N. H., Dang H. L., Hoxha D., Closed-form solution of stress state and stability analysis of wellbore in anisotropic permeable rocks, Int J Rock Mech Min Sci, 113, 2019, pp. 11-23.

[10] Tran N. H., Do D. P., Vu M. N., Nguyen T. T. N., Pham D. T., Trieu H. T., Combined effect of anisotropy and uncertainty on the safe mud pressure window of horizontal wellbore drilled in anisotropic saturated rock, Int J Rock Mech Min Sci 152, 2022, pp. 1-20.

[11] Khoshghalb A. & Khalili N., A meshfree method

for fully coupled analysis of flow and deformation in unsaturated porous media, Int. J. Numer. Anal. Meth. Geomech., 37 (2013), pp. 716-743.

[12] Khoshghalb A. & Khalili N., An alternative approach for quasi-static large deformation analysis of saturated porous media using meshfree method, Int. J. Numer. Anal. Meth. Geomech., 39(2015), 913-936.

[13] Ghaffaripour O., Esgandani G. A., Khoshghalb A. & Shahbodaghkhan B., Fully coupled elastoplastic hydro-mechanical analysis of unsaturated porous media using a meshfree method, Int. J. Numer. Anal. Meth. Geomech., 43(2019), 1919-1955.

[14] Shafee A. & Khoshghalb A., An improved node-based smoothed point interpolation method for coupled hydro-mechanical problems in geomechanics, Computers and Geotechnics, 139 (2021), 104415.

[15] Abousleiman Y., Ekbote S., Solutions for the inclined borehole in a porothermoelastic transversely isotropic medium, J Appl Mech 72, 2005, pp. 102–114.

[16] Kanfar M. F., Chen Z., Rhaman S. S., Fully coupled 3D anisotropic conductive-convective porothermoelasticity modeling for inclined boreholes, Geothermics, 61, 2016, pp. 135–148.

[17] Cui Y. J., Sultan N. & Delage P., A thermomechanical model for saturated clays, Canadian Geotechnical Journal, 37(2000), 607-620.

[18] Shahbodagh B., Habte M. A., Khoshghalb A. & Khalili N., A bounding surface elasto-viscoplastic constitutive model for non-isothermal cyclic analysis of asphaltic materials, Int. J. Numer. Anal. Meth. Geomech., 41(2017), 721-739.

[19] Roland W. L., Perumal N., Seetharamu K. N., Fundamentals of the finite element method for heat and fluid flow, Wiley, 2004, pp. 5-12.

[20] Ghassemi A., Diek A., Porothermoelasticity for swelling shales, J Pet Sci Eng, 34, 2002, pp.123–135.

[21] Granet S., Modelings THHM: General information and algorithms, 2014, https://code-aster.org/V2/doc/default/en/man_r/r7/r7.01.10.pdf , pp. 1-32.

[22] Tran N. H., Nguyen T. T. N., Pham D. T., Trieu H. T., Thermo-hydro-mechanical responses of the host rock in the context of geological nuclear waste disposal, J Appl Sci Eng, 26 (12), 2023, pp. 1689–1702.

[23] Aadnøy B. S., Looyeh R., Petroleum rock mechanics, Drilling operations and well design, 2nd ed., Gulf Professional Publishing-Elsevier, 2019, pp. 131-245.